JCTC Journal of Chemical Theory and Computation

Vibrational Spectra of Small Protonated Peptides from Finite Temperature MD Simulations and IRMPD Spectroscopy

A. Cimas,[†] T. D. Vaden,*[,‡] T. S. J. A. de Boer,[‡] L. C. Snoek,[‡] and M.-P. Gaigeot*[,†]

LAMBE UMR8587 Laboratoire Analyse et Modélisation pour la Biologie et l'Environnement, Université d'Evry val d'Essonne, Blvd F. Mitterrand, Bât. Maupertuis, 91025 Evry, France, and Physical and Theoretical Chemistry Laboratory, Chemistry Department, University of Oxford, South Parks Road, Oxford OX1 3QZ, United Kingdom

Received February 1, 2009

Abstract: Finite temperature Born−Oppenheimer DFT-based molecular dynamics simulations are presented for the vibrational spectroscopy of the prototype gas-phase Ala_2H^+ and Ala_3H^+ protonated peptides. The dynamics and the vibrational signatures are used to interpret IR-MPD spectra recorded in the NH/OH stretch region. Molecular dynamics simulations are one way to go beyond the harmonic approximations commonly applied for the calculations of infrared spectra, naturally including all anharmonicities, i.e. mode couplings, vibrational and dipole anharmonicities. The dynamics of the peptides allows understanding of the evolution of the shape and width of the N−H bands when increasing the size of the peptide, as demonstrated here with the two small prototypes Ala_2H^+ and Ala_3H^+. Hence, the conformational dynamics of Ala_2^+ at room temperature participates to the broadening of the IR active bands. The complex N−H broadband of Ala_3H^+ is shown to result from the dynamics of the N−H groups in the different peptide families, with a special role from breaking/reforming of hydrogen bonds involving the N−H groups. Taking this dynamics into account is thus mandatory for the understanding of this band in the 300−400 K experimental spectrum.

Introduction

Characterizing the folding behavior of peptide chains is of fundamental importance for a better understanding of proteins. The conformational structures and dynamics of simple model oligopeptides have been studied in solution by NMR and 2-D IR spectroscopy,[1−3] but the role of the aqueous environment on peptide behavior is an open question. The intrinsic peptide structures and dynamics may be explored in the gas phase, where the solution environment is removed and the folding behavior is determined exclusively from the noncovalent interactions associated with the peptide backbones and/or side chains. This has catalyzed many structural investigations of cold, gas-phase peptides, revealing gas-phase formation of traditional secondary-structure motifs like helices, β-sheets, and β- and γ-turns.[4−9]

For a complete picture of folding behavior in gas-phase oligopeptides it is necessary to include the effects of temperature. At physiological temperatures, entropic differences between conformations can alter the free energy surfaces, and as a result multiple conformational families may be populated and barriers to conformational isomerization may be surmounted. While frozen peptides at 0 K exhibit only one or a few distinct structures, at 298 K peptides are better described in terms of average conformation(s), with a (relatively) rigid backbone and moderate or large-amplitude side-chain motions.[10] The motivation to understand these issues is reflected in the work of Polfer et al.[11] and Gregoire et al.,[12] in which protonated peptide ions are characterized at ∼300 K using Infrared Multiple Photodissociation (IR-

* Corresponding author e-mail: timothy.vaden@chem.ox.ac.uk (T.D.V.), mgaigeot@univ-evry.fr (M.-P.G.).

[†] Université d'Evry val d'Essonne.

[‡] University of Oxford.

10.1021/ct900057s CCC: $40.75
Published on Web 03/20/2009

MPD) spectroscopy with a Free Electron Laser (FEL). Vaden et al. have recently investigated protonated polyalanine peptides, Ala_nH^+, under elevated internal energy conditions by generating the ions via UV photochemical protonation.[13] The 'temperature' of the ions produced in these experiments is roughly estimated about 350 K, so that the peptides structural and dynamical properties extracted from these experiments are relevant for understanding the room temperature physiological medium. When turning to theoretical calculations in order to interpret the IR-MPD recorded features, one should be aware that the local dynamics of the peptides (e.g., hydrogen bonds dynamics, methyl groups rotation, local distortions of the peptide chain) and the conformational isomerization/interconversion dynamics of the peptides as well as anharmonic vibrational effects (i.e., mode couplings, vibrational and dipole anharmonicities) may be pivotal issues for the comprehension of the finite temperature experimental vibrational features. See our recent papers[12,14,15] on these issues.

The dynamics of the molecules (local or more global isomerization/interconversion) and their direct consequences on measured properties such as vibrational spectra can only be accounted for through molecular dynamics (MD) simulations.[16,17] The calculation of infrared spectra through MD relies on dipole time correlation functions recorded along a trajectory.[18] This is well established in the context of classical MD[19−24] but is much more recent in the ab initio MD community. Pioneering studies were done by Parrinello et al. on liquid water,[25−27] and within the past few years, we have shown that ab initio molecular dynamics represents the best method for the calculation of IR spectra of DNA and peptide building blocks in the gas phase or immersed in liquid water[12,14,15,28−30] at room temperature. We have in particular shown that ab initio MD simulations are the proper tool to calculate IR absorption spectra of gas-phase molecules that can exist in multiple isomeric conformations at finite temperature.[14]

Another advantage of MD simulations for the calculation of IR spectra is that vibrational anharmonicities are directly taken into account in the final spectrum. The two successive harmonic approximations usually adopted for the determination of IR spectra from static ab initio calculations, i.e. a harmonic approximation of the potential energy surface at the optimized geometries and a mechanical harmonic approximation for the transition dipole moments, are omitted in MD, because they are not needed. Hence, the finite temperature dynamics take place on all accessible parts of the potential energy surface, be they harmonic or anharmonic. As the calculation of IR spectra with MD is related only to the time-dependent dipole moment, it does not require any harmonic expansion of the transition dipole moments. Therefore, if the dipole moments and their fluctuations are accurately calculated along the trajectory, the resulting IR spectrum should be reliable too, as demonstrated in our previous works.[12,14,28−30] Furthermore, the temperature and the conformational dynamics of the peptide will contribute to vibrational band broadening.

In this article, we apply DFT-based Born−Oppenheimer dynamics at ∼300−400 K on the prototype gas-phase alanine protonated di- and tri-peptides in order to calculate their infrared spectral signatures. Our goal is to interpret the vibrational features at the microscopic level, with a special emphasis on the evolution of the active bands with the peptide size increase. The dynamics and the vibrational signatures are then used to interpret IR-MPD spectra recorded in the NH/OH stretch region. We have chosen these two well-studied small protonated polyalanines (see for instance refs 13 and 31) in order to demonstrate that the peptides dynamical features have to be taken into account to obtain a precise understanding of the relation between experimental features and the underlying molecular structural and dynamical properties, including anharmonicities. Previous investigations reported in the literature on these systems[13,31,32] have combined IR-MPD spectra in the NH/OH or mid-IR amide domains and scaled harmonic DFT frequencies computed for frozen conformations of the peptides, thereby neglecting vibrational anharmonic contributions and local/nonlocal conformational dynamics at the finite temperature of the experiments. The present investigation goes beyond these approximations. Note that these issues have already been addressed on Ala_2H^+ with DFT-based Car−Parrinello modeling in the mid-IR region.[12,14]

IR-MPD Setup

The experimental method and experimental results are unchanged from our previous Ala_nH^+ investigation.[13] The following brief description is given for a better assessment of the interplay between the experiments and the theoretical investigations. Ala_2H^+ and Ala_3H^+ ions were generated by a photochemical protonation scheme (1)−(4), described in detail elsewhere,[33−35] in which intermolecular proton transfer follows resonance-enhanced 2-photon ionization (R2PI) of a phenol-peptide ($PhOH..Ala_n$, $n = 2,3$) complex.

$$PhOH + Ala_n \rightarrow [PhOH..Ala_n] \quad (1)$$

$$[PhOH..Ala_n] + 2h\nu \rightarrow [PhOH^+..Ala_n]^{\bullet} \quad (2)$$

$$[PhOH^+..Ala_n]^{\bullet} \rightarrow PhO^{\bullet}..Ala_nH^+ \quad (3)$$

$$PhO^{\bullet}..Ala_nH^+ \rightarrow PhO^{\bullet} + Ala_nH^+ \quad (4)$$

Cold $PhOH..Ala_n$ complexes were generated, step (1), by seeding gas-phase Ala_n peptides (using laser desorption by a Continuum Minilite Nd:YAG laser) into a pulsed supersonic expansion of phenol in argon carrier gas. The complexes passed through a skimmer into the extraction region of a linear time-of-flight (TOF) mass spectrometer (R. M. Jordan), where they were ionized, step (2), at ∼278 nm via R2PI using the frequency-doubled output of a Lamda-Physik FL2002 dye laser. Rapid, exothermic proton transfer within the ionized complexes, $[PhOH^+..Ala_n]^{\bullet}$, step (3), followed by endothermic loss of the phenoxy radical $PhO^{\bullet}$, step (4), generated the free protonated peptide ions, Ala_nH^+. Ala_2 samples were obtained from Aldrich, while Ala_3 samples were obtained from Bachem (Germany).

The internal energy content of the protonated cations depends on the excess energy after two-photon ionization

(~60 kJ.mol^{-1}), the ΔH of the proton transfer reaction (3) (~100 kJ.mol^{-1}), and the binding energy of the $PhO^{\bullet}..Ala_nH^+$ complex (estimated to be ~75 kJ.mol^{-1}).[33] As discussed previously, the 'temperatures' of the $Ala_{2,3}H^+$ ions, which depend on the peptide size through the vibrational heat capacities, are not well-characterized but could be anywhere from 250 K to more than 400 K.[13] Previous analyses have assumed temperatures of 350 K as a rough guide, but in the current work we consider several different temperatures, enabling a better characterization of the internal energy content.

The $Ala_{2,3}H^+$ ions were probed with IR-MPD spectroscopy using the idler output (~10−20 mJ/pulse, tunable from 2000−4000 cm^{-1}, with a bandwidth of ~2 cm^{-1}) of a LaserVision KTP/KTA OPO/OPA laser system, tightly focused to a beam diameter ~800 μm, which intersected the ions 400 ns after the UV pulse, in a spatially distinct region downstream from the ionizing UV laser beam. IR-MPD spectra were recorded by monitoring the depletion of the (parent) protonated peptide ion (using active baseline correction[13]) as a function of the IR frequency, since the TOF mass spectra were too congested to unambiguously identify the fragment ions.

DFT-Based Molecular Dynamics

We perform Born−Oppenheimer molecular dynamics simulations (BOMD) with the CP2K package,[36,37] where nuclei are treated classically and electrons quantum mechanically within the DFT (Density Functional Theory) formalism. These simulations solve Newton's equations of motion of the nuclei at finite temperature, while the electronic wave function is obtained at each nucleus conformation by solving the time-independent Schrödinger equation. Forces that act on the nuclei are derived from the Kohn−Sham energy. Details on the molecular dynamics setup are presented in the Supporting Information. Briefly, we use the Becke, Lee, Yang, and Parr (BLYP) gradient-corrected functional[38,39] and Goedecker-Teter-Hutter (GTH) pseudopotentials.[40−42] A double-ζ (DZVP) Gaussian basis set (from the CP2K library) and a 320 Ryd Plane-wave density cutoff have been applied. With this basis set the four structures of Ala_2H^+ from ref 32 have been reoptimized and are found in the same energy order and with similar energy gaps as in refs 14 and 32 i.e. transA1 (least energy), transO1 (+1.32 kcal/mol), transA2 (+1.72 kcal/mol), and cisA3 (+2.57 kcal/mol), with the Zero Point Energy (ZPE) included. Note that the use of a bigger plane-wave basis set in ref 14 led to the energy inversion of conformers transO1 and transA2. The Ala_3H^+ two main conformers identified as $A_3$1 and $A_3$3 in ref 13 with an energy gap of 4.88 kcal/mol from DFT/B3LYP/6−31+G(d,p) optimizations is found at 3.83 kcal/mol with the present BLYP/DZVP optimization, including the ZPE. The BLYP/DZVP present method thus gives similar minima and energy gaps on the potential energy surfaces of Ala_2H^+ and Ala_3H^+ protonated peptides as with e.g. B3LYP and more extended basis sets. In any case, the use of diffuse functions is less critical in charged species.

The dynamics are performed in the microcanonical NVE ensemble (after an equilibration period, see details in the Supporting Information) with a time-step of 0.5 fs. With BOMD, discrepancies between calculation and experiment are expected to be due to the choice of the DFT functional (BLYP throughout this paper), as DFT-based dynamics are only as good as the functional itself allows.

Calculation of the IR absorption coefficient $\alpha(\omega)$ by means of MD makes use of the relation derived from Linear Response Theory involving the Fourier Transform of the dipole time correlation function,[18] as described in our previous works[12,14,28−30]

$$\alpha(\omega) = \frac{2\pi\beta\omega^2}{3n(\omega)cV} \times \int_{-\infty}^{\infty} dt \ \langle \mathbf{M}(t)\cdot\mathbf{M}(0)\rangle \exp(i\omega t) \quad (5)$$

where $\beta = 1/kT$, $n(\omega)$ is the refractive index, c is the speed of light in vacuum, and V is the volume. $\mathbf{M}$ is the total dipole moment of the system, which is the sum of the ionic and electronic contribution.[26] Interpretation of the infrared-active bands into individual atomic displacements is done with the vibrational density of states (VDOS) formalism. This is obtained by Fourier transformation of the atomic velocity autocorrelation functions and is decomposed into individual atomic contributions or into groups of atoms.[30] Note that we do not apply any scaling factor to the vibrational band positions extracted from our calculations.

Setup of the Dynamics

We performed three separate dynamics of the protonated Ala_2H^+ dipeptide and eight dynamics of the protonated Ala_3H^+ tripeptide. The trajectories of Ala_2H^+ span a total 30 ps dynamics, where the average temperature is 290 ± 37 K. The initial configurations (positions and velocities of the atoms) of the dynamics have been taken from the end of the dynamics reported in our previous work.[14] The trajectories of Ala_3H^+ also span a total ~30 ps dynamics with temperatures ranging between 387 ± 38 K and 530 ± 50 K, on average; choice of the temperatures will be explained below. The molecular dynamics simulations of the protonated tripeptide follow our general two-steps setup, i.e. an equilibration phase of 1−3 ps with a control of temperature through velocity rescaling, followed by data collection over trajectories in the microcanonical ensemble (no rescaling of velocities), each one for 3.2−3.7 ps.

We have considered three families of the Ala_3H^+ tripeptide in our ab initio dynamics simulations, as illustrated in Figure 1. The dynamics were initiated from optimized structures found in our previous work[13] (labeled $A_3$1, $A_3$3, and $A_3$5). $A_3$1 and $A_3$3 are the two structures found lower in energy[13,31] in previous works, with their relative energy that depends on the ab initio level of theory (DFT and MP2) and basis set used in the optimization procedures. The family hereafter denoted 'NH_2' corresponds to a tripeptide in which the proton is located on the N-terminal carbonyl group and is initiated from the $A_3$1 optimized conformation of our previous work.[13] The supplementary proton of the family hereafter denoted 'elongated NH_3^+' (or simply 'NH_3^+') is located on the N-terminal NH_3^+ and displays an extended peptide chain, and the dynamics of this family are initiated from the $A_3$5 optimized conformation. This structure lies higher in energy

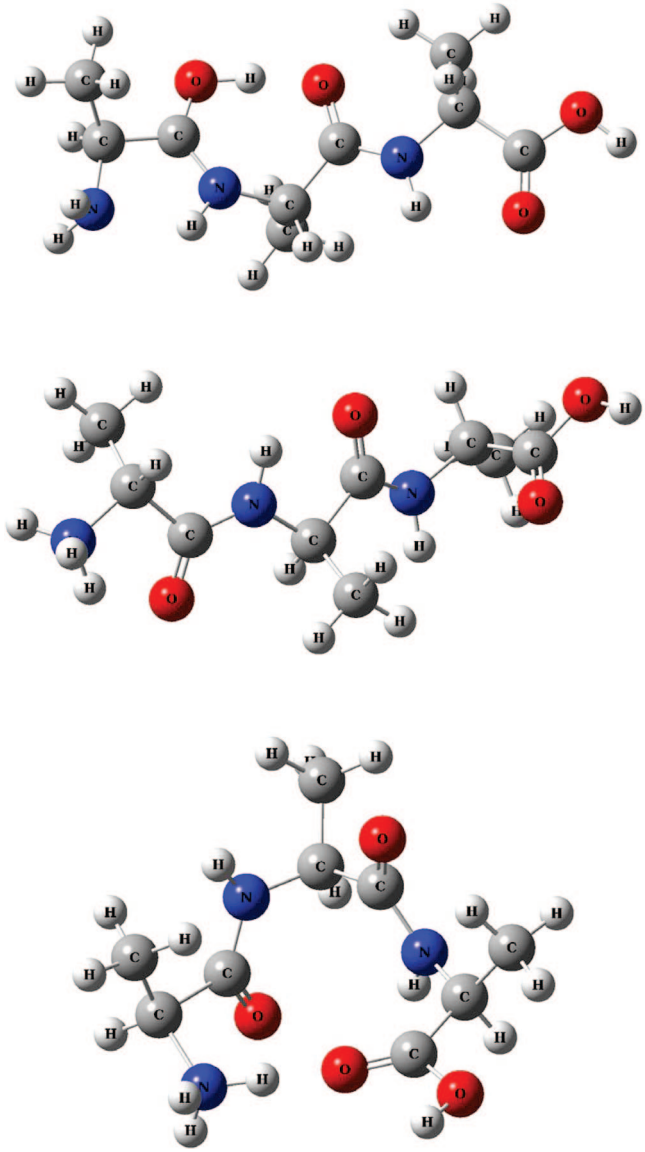

Figure 1. Schematic representation of the main structures of Ala_3H^+ which have been used as initial structures in the DFT-based Born−Oppenheimer dynamics. From top to bottom: NH_2 family, elongated NH_3^+ family, and folded NH_3^+ family. Carbon atoms are represented in dark gray, nitrogen atoms in dark blue, oxygen atoms in red, and hydrogen atoms in light gray.

than the A_31 and A_33 ones[13,31] and was therefore discarded in the previous analysis of the IR-MPD spectra. We have nonetheless investigated this type of conformer in the present work, considering that it could be populated as a result of the method of production of the ions in the present experiment where a photochemical scheme is employed. The other reason is that this conformation is very similar to the one of the Ala_2H^+ that was observed in our previous MD work.[14] The third family investigated is denoted 'folded NH_3^+' (or simply 'folded') and corresponds to a folded chain through a $NH_3^+\cdots O{=}C$ H-bond and is initiated from the A_33 optimized conformation of our previous work.[13]

Two dynamics of the NH_2 family have been performed at 380 ± 36 K and two other dynamics at 460 ± 40 K and 530 ± 50 K, respectively. Two dynamics of the NH_3^+ family have been performed at 380 ± 37 K and a supplementary dynamics at 450 ± 45 K. The trajectory of the folded family has been performed at 400 ± 40 K. The dynamics performed at higher temperatures were begun from the end of lower temperature dynamics, heated up and equilibrated for 2−3 ps, and then evolved in the microcanonical ensemble. As already emphasized, the exact value of the temperature in the related IR-MPD experiments is not well-characterized but roughly estimated about 350 K, thus the average 380−400 K achieved in the dynamics performed on Ala_3H^+. The highest temperatures chosen here are aimed at investigating the temperature effect on the final vibrational features. The final spectra of Ala_2H^+ and of Ala_3H^+ presented here have been averaged over all performed trajectories.

One has to be cautious when trying to compare the calculated IR absorption intensities (calculated within the static or the dynamics formalisms) to those obtained in IR-MPD experiments. Equation 5 is strictly valid for one-photon linear IR absorption spectroscopy. IR-MPD on the other hand is a multiphotonic process leading to the fragmentation of the molecule. The recorded signal is the fragmentation yield with respect to each excitation IR wavelength. It is thus an indirect measurement of IR absorption, in contrast to the usual linear IR spectroscopy. Calculations and experiments are therefore not directly comparable where band intensities are concerned, thereby displaying expected discrepancies. The direct simulation of IR-MPD spectra, with a clear theoretical expression of the signal in terms of dynamical quantities, remains an unsolved problem. Comparisons of experimental and calculated IR intensities will therefore be cautiously discussed in the following analyses.

Structural Analyses along the Trajectories

Ala_2H^+. The dynamics of the protonated Ala_2H^+ dipeptide using DFT-based Car−Parrinello molecular dynamics simulations have already been presented and discussed in our previous work,[14] though in another context. The same dynamical results are obtained here, despite the changes in the dynamical approach (Born−Oppenheimer versus Car−Parrinello) and the basis set representation between the two works. Briefly, the protonated dipeptide undergoes continuous conformational dynamics at room temperature between transA1 and transA2 conformers (see ref 14 for more details about the nomenclature adopted for the isomers). This conformational dynamics corresponds to the $N-C-C_\alpha-O$ torsional rotation of the C-terminal COOH of the peptide, without energy barrier.[14] We also observe proton transfers between the NH_3^+ N-terminal and the neighboring carbonyl on the chain, giving rise to transient periods of time during which the transO1 conformer (NH_2/COH) is populated.[14] Overall, conformations where the N-terminal of the peptide is protonated (NH_3^+) are predominantly populated, with a strong hydrogen bond that is formed between NH_3^+ and the neighboring carbonyl group. Moreover, there is enough energy for the NH_3^+ group to rotate and exchange the hydrogen atom that can be hydrogen bonded to the neighboring carbonyl.

We find that, depending on the orientation of the C-terminal COOH during the dynamics, the amide N−H group

can be located in the vicinity of the carbonyl group of COOH with an average N−H···O═C distance of ∼2.1 Å or away from it with distances of the order of ∼3.2−3.5 Å. The short ∼2.1 Å distances cannot be classified as proper hydrogen bonds, since the corresponding average N−H···O angles of ∼110° are too far from the ideal linearity. Considering the geometrical hindrances of the peptide chain, improper hydrogen bonds between neighboring groups on the chain are expected to occur. We observe that the C-terminal O−H group is never involved in any hydrogen bond and thus remains free over the dynamics. Finally, there is not enough energy in the system to overcome the energy barrier of the trans/cis orientation of the peptide bond.

Ala_3H^+. The two dynamics of the NH_2 family performed at 380 K give rise to the exploration of helical α_L conformations of Ala_3H^+, where Φ (Φ = C1−N−C_α−C2 where C1 is the N-terminal carbonyl atom and C2 is the C-terminal carbonyl atom) and Ψ (Ψ = N1−C_α−C2−N2 where N1 is the N-terminal amide nitrogen atom and N2 is the C-terminal amide nitrogen atom) angles are in the [0/100°] and [100/180°] domains, while the dynamics performed at higher temperatures explore either exclusively helical α_R conformations with Φ and Ψ angles, respectively, in the [0/−100°] and [−100/−180°] domains for the 460 K dynamics or a mixture of α_L and α_R conformations for the higher 530 K temperature dynamics. There is therefore a transition between α_L and α_R conformations of the protonated tripeptide that becomes permitted with the increase of the temperature for the NH_2 family (at least within the time-lengths of the simulations performed here). All dynamics on the NH_3^+ family explore the [90−180°] domain of Φ and both [150−180°] and [−150/−180°] domains of Ψ, which also grossly correspond to helical α_L and α_R conformations of the tripeptide. The domains explored by the folded peptide correspond to [−100/−50°] and [60/130°], respectively, for Φ and Ψ, which is the domain of the polyproline PII structure. As already observed for the Ala_2H^+ dipeptide, the C-terminal COOH of the elongated Ala_3H^+ tripeptide undergoes a rotational motion without energy barrier.

Overall, we do not observe spontaneous conformational interconversion/isomerization of Ala_3H^+ during the dynamics close to room temperature. This becomes permitted around 500 K.

The dynamics of the NH_2 family display an equal population of conformations where there is an attraction between NH_2 and the neighboring backbone amide N−H, which gives rise to an average H_2N···H−N distance of ∼2.1 Å, and population of conformations where there is no attraction between NH_2 and the neighboring amide N−H, as revealed by H_2N···H−N distances above 2.5 Å. The short average H_2N···H−N distance of ∼2.1 Å is associated with an average value of the N−H···N angle of ∼110−120°, which does not characterize N−H···N as a proper H-bond. The attraction between the two groups is nonetheless sufficient to induce an increase of the amide N−H bond length to ∼1.05 Å (∼0.02 Å longer than the average C-terminal N−H amide). The H_2N···H−N can be viewed as an energetically weak H-bond. Therefore, the dynamics of the NH_2 family of the tripeptide display an equal

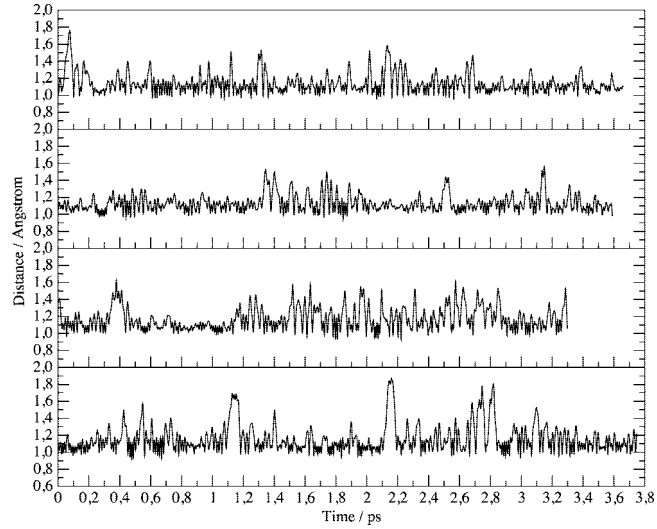

Figure 2. Time evolution of the distance C1−O1−H···O2═C2 for the four dynamics of the NH_2 family of Ala_3H^+ performed in this work, where C1 is the N-terminal carbonyl and C2 is the C-terminal carbonyl. The distance is reported with O1 as the reference.

population of conformations where a weak H_2N···H−N H-bond is formed and where this weak H-bond is broken. Breaking and reforming of this H-bond is observed along all the dynamics performed here.

We have illustrated in Figure 2 the evolution with time of the C−O−H···O═C distance in the NH_2 tripeptide family. Though the supplementary proton of the protonated peptide can be seen hopping between both oxygen sites, it is mainly shared between the two carbonyl groups of the tripeptide with an average H···O distance of ∼1.10−1.13 Å. We can distinguish periods of times during which the supplementary proton is located on the N-terminal C═O (O−H ∼1.0 Å) and other periods of times during which it is located on the C-terminal C═O (which appear as transient and short time spans), but the average localization of the proton is mainly seen in between the two carbonyl groups.

Interestingly, the dynamics of the protonated tripeptide in which the proton is located on the N-terminal NH_3^+ at the beginning of the simulation give rise to the exploration of proton transfer events between the NH_3^+ extremity and the neighboring carbonyl group, as illustrated in Figure 3 where we have reported the evolution with time of the distance NH_3^+···O═C along the three dynamics performed in this work. The supplementary proton either remains at the NH_3^+ terminal giving rise to a strong hydrogen bond between NH_3^+ and the neighboring carbonyl group, with an average NH_3^+···O═C distance of 1.6−1.7 Å, or jumps to the neighboring carbonyl group thus forming an N-terminal amine NH_2 and a protonated C−O−H. The C−O−H remains H-bonded to the amine, with an average C−O−H···N−H distance of 1.6−1.7 Å and an average angle of 130−140°. Note that as observed for Ala_2H^+, there is also enough energy for the NH_3^+ extremity of Ala_3H^+ to rotate and exchange the hydrogen atom that can be hydrogen bonded to the neighboring carbonyl, as can be seen from Figure 3 (bottom). The proton transfer thus proceeds without any energy barrier at the temperature of the simulations performed in the present

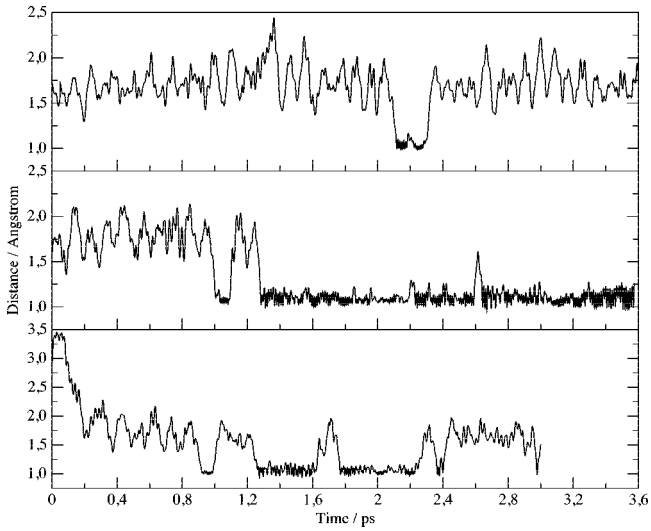

Figure 3. Time evolution of the distance (N-)$H^+\cdots O1{=}C1$ for the three dynamics of the NH_3^+ family of Ala_3H^+ performed in this work. $N{-}H^+$ is one group of the N-terminal NH_3^+.

work. Overall, the configurations protonated at the N-terminus are observed predominantly, but longer statistics would be needed in order to give a more definite statement. The C-terminal N−H and C═O groups form a weak distorted H-bond, with an average distance of 1.9−2.0 Å and an average N−H···O═C angle of 120−130°.

In the case of the folded NH_3^+ family, the dynamics at 400 K shows that there is a rotational motion of the NH_3^+ N-terminal which induces alternate periods of times during which a $NH_3^+\cdots O{=}C$ H-bond between both N- and C-terminal extremities of the folded peptide can be observed and periods of times during which this H-bond is broken. As a consequence, the dynamics explore, on average, an equal percentage of conformations displaying a $NH_3^+\cdots O{=}C$ H-bond between both N-terminal and C-terminal extremities of the folded peptide and of conformations in which this H-bond is lost. We note that the H-bonds are formed for ∼100 fs before breaking again. The $NH_3^+\cdots O{=}C$ H-bond is therefore not energetically strong. As a consequence of the rotation of the NH_3^+, there is formation and breaking of a hydrogen bond between NH_3^+ and the neighboring C═O carbonyl located at the N-terminal of the chain. These two H-bonds can be viewed, on average, to replace each other, while the NH_3^+ rotates. The N-terminal C═O does not form a H-bond with the C-terminal amide N−H, as they are on average apart from each other by ∼2.8 Å. Variations are observed for the dihedral angles around the central $N{-}C_\alpha$ and $C_\alpha{-}C$ bonds (variations by ∼60°), which indicate that the skeleton of the folded Ala_3H^+ presumably tries (unsuccessfully) to slightly unfold.

Methyl groups rotate freely along all the dynamics performed, with the amplitude of the $(H_3)C{-}C_\alpha{-}C{-}N$ dihedral angles varying by up to ∼80°. All the peptide groups remain in their trans orientation along all the simulations. The trans/cis peptide bond isomerization barrier is generally estimated as a few tens of kcal.mol $^{-1}$,[32,43,44] and it is too high to be observed spontaneously at the temperatures of the dynamics of the present work.

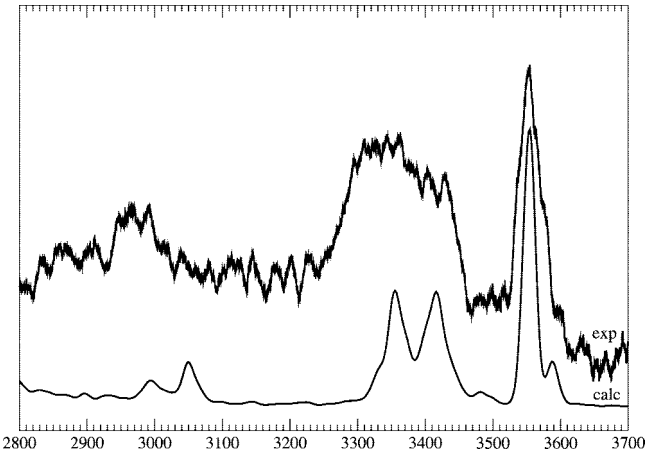

Figure 4. Comparison of the experimental infrared spectrum of Ala_2H^+ (top, from ref 13) and the calculated spectra from DFT-based Born−Oppenheimer dynamics at room temperature (bottom).

Infrared Spectroscopy

Infrared Spectroscopy of Ala_2H^+. The infrared spectrum of the gas phase Ala_2H^+ calculated from our trajectories, superimposed with the experiment, is presented in Figure 4. The theoretical spectrum has been averaged over the three trajectories performed in this work, corresponding to a total of 30 ps dynamics.

It must be emphasized that each of the three dynamics gives different individual active IR features of the protonated dipeptide, depending on the underlying dynamical behavior of the molecule, e.g., depending on the relative population of transA1 or transA2 conformations explored along the trajectories, or the appearance of transO1 conformations along the trajectories. Temperature and conformational dynamics naturally give rise to the breadth of the vibrational bands, without applying any empirical model. Note that the intensities of the calculated bands have been normalized with respect to the experimental 3560 cm^{-1} band. We can see that our calculation then reproduces the intensities of the two other bands very well, even though the linear IR theoretical signal and the IR-MPD experimental signal are not fully comparable, see the Introduction. Our calculations do not make any assumptions about harmonic modes or harmonic dipoles: all anharmonicities are naturally taken into account in the theoretical spectrum. Furthermore, no frequency scaling factors nor translations have been applied to the calculated spectrum. The remaining band shifts with respect to experiment are therefore the result of a combination of the ab initio method (DFT) and the basis set (DZVP) used.

The band located at 3560 cm^{-1} corresponds to the O−H stretch of the C-terminal COOH group of the dipeptide. The calculation matches the experimental band in terms of position and band shape. The shoulder located at ∼3590 cm^{-1} nicely reflects the feature present in the experimental spectrum.

The broadband located between 3300 and 3500 cm^{-1} (including the small feature at ∼3490 cm^{-1}) can be assigned

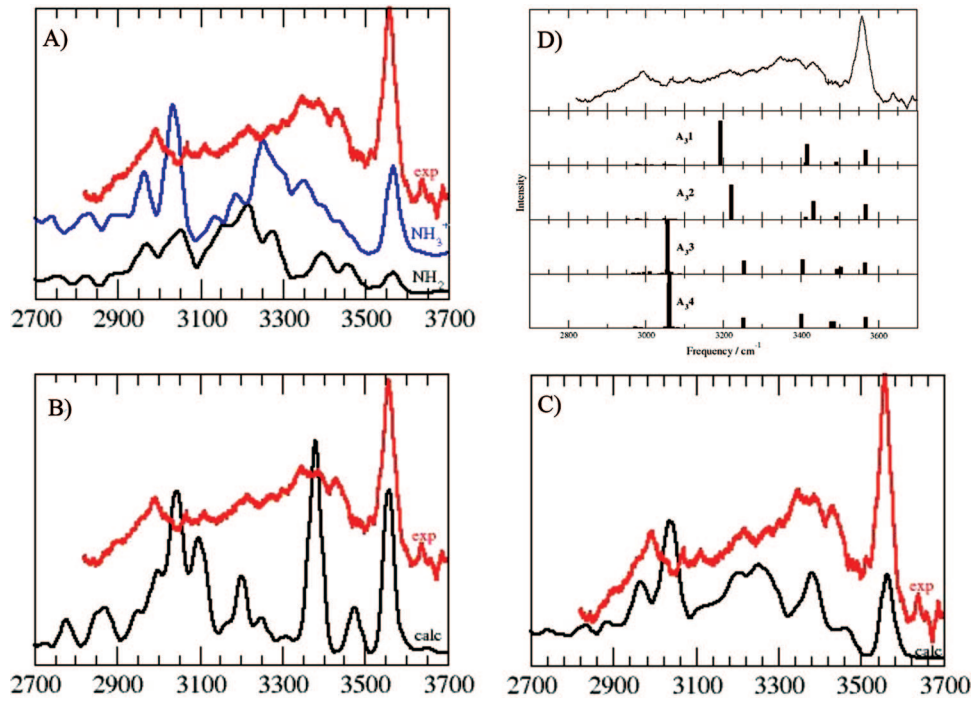

Figure 5. (A-C) Infrared spectra of Ala_3H^+ calculated from DFT-based Born−Oppenheimer dynamics. The spectra are plotted in relation to the conformational families of the tripeptide explored during the trajectories (see text for explanations). The spectra presented for each family have been averaged over the performed dynamics. A: NH_2 (black line) and NH_3^+ (blue line) families; B: folded family (black line); C: the final infrared spectrum of Ala_3H^+ (black line) averaged over all the trajectories performed in this work. Experiment (in red in all graphs) is from ref 13. D: Scaled harmonic frequencies obtained for the four optimized geometries of Ala_3H^+ as obtained in ref 13.

to the N−H stretches from the amide N−H group and from the free N−H groups of the NH_3^+ N-terminal. The symmetric and antisymmetric stretches of the free N−H of the NH_3^+ can be seen at 3415 and 3370 cm^{-1}, respectively, under the broad experimental band. The backbone amide N−H stretch also appears on the higher frequency part of the band, around 3415 cm^{-1}. Although the calculated band nicely reflects the two parts which can be observed in the experimental band, it is nonetheless not broad enough in comparison to the experiment. The breadth of the IR bands in molecular dynamics results from the temperature, conformational dynamics of the molecule, and anharmonicities. The difference observed here may be the signature that the temperature of the simulations is not high enough and that the experiments are indeed performed at a higher temperature. Interestingly, the IR signature of NH_3^+ that is hydrogen bonded to the neighboring C═O carbonyl throughout the simulations is spread over the broad 2500−2850 cm^{-1} region of the spectrum (not shown), thus strongly shifted down from the symmetric and antisymmetric modes of NH_3^+. Strong anharmonicity of the N−H···O═C hydrogen bond is responsible for the *displacement* of this band, whereas anharmonicity and the dynamics of the hydrogen bond at finite temperature are responsible for its *width*. Indeed, the N−H^+···O═C H-bond distance fluctuates by 0.3−0.4 Å around its mean value, and there is enough energy for the NH_3^+ group to rotate and exchange the hydrogen atom which can be hydrogen bonded to the neighboring carbonyl. These complex H-bond dynamics therefore lead to vibrational signatures which are spread over a large frequency domain. Note that our previous harmonic calculations[34] on Ala_2H^+ neglected this point. This is where finite-temperature molecular dynamics simulations are very useful for the calculation of vibrational spectra, as they are not restricted to the harmonic approximations of the modes.

The third double band of the IR spectrum in the investigated 2800−4000 cm^{-1} region is related to combined C_α−H and C−H stretch modes of the methyl groups of the peptide. These bands are shifted to higher frequency relative to the experiment by ∼40 cm^{-1}, and the band spacing between the two bands (∼50 cm^{-1}) is slightly bigger than the experimental one (∼30 cm^{-1}). It is nonetheless remarkable that our calculation predicts an intensity of the band so close to the experiment. Again, the harmonic calculation[34] does not give such intensity to this mode.

Infrared Spectroscopy of Ala_3H^+. Spectra of the protonated alanine tripeptide obtained from the ab initio trajectories are presented in Figure 5. The spectra are plotted in relation with the conformational families of the tripeptide explored during the trajectories: (*i*) the NH_2 family where the supplementary proton is located on the N-terminal carbonyl group, the N-terminal NH_2 displaying an equal population of conformations of weak H_2N···H−N hydrogen bonds and without any such hydrogen bonds, (*ii*) the NH_3^+ family where the supplementary proton is predominantly located on the N-terminal NH_3^+ but can transfer to the neighboring carbonyl during the dynamics, and (*iii*) the folded family where the peptide chain is folded through a weak NH_3^+···O═C H-bond, which has been shown to break/reform during the dynamics. The spectra presented for each family have been averaged over the corresponding dynamics

(apart from family (*iii*) where only one trajectory has been performed). See Figure 5-A and -B for the results presented individually for each family. The final spectrum of Ala_3H^+, presented in Figure 5-C, has been averaged over all the trajectories performed for this molecule. Considering the production method of the ions in the associated experiments, which certainly does not follow a thermalized Boltzmann distribution, such an average in the calculation appears reasonable. In the following, we will mainly concentrate our discussion on the band-positions and the band-shapes of the theoretical spectra in comparison to the experimental spectrum, as again intensities of the calculated spectra and the experimental IR-MPD signals are not strictly identical.

As has already been emphasized for the protonated dipeptide, each dynamics within a conformational family gives different individual active IR features, depending on the underlying dynamical behavior of the molecule at the temperature of the simulations (room temperature and above). At finite temperature, the statistical average of the spectra is meaningful and can thus be compared to the spectrum recorded in the experiment. Temperature and the conformational dynamics of the peptide will induce the broadening of the vibrational bands. Vibrational anharmonicities explored at this temperature, i.e. anharmonicity from the potential energy surface and from the molecular dipole, will induce band shifts and also participate in the broadening of the bands.

The experimental spectrum[13] is reported in all figures. All the spectra display the same vibrational patterns that will be discussed below, whatever the tripeptide family they are related to. The position, intensity, and shape of the individual bands will slightly change depending on the trajectory and the Ala_3H^+ family that is concerned, but the assignments of the bands are maintained. In the following, we discuss the bands of the average spectrum (Figure 5-C) and extract the vibrational assignments from the individual trajectories.

The band located at 3560 cm^{-1} corresponds to the O−H stretch of the C-terminus. As expected from the similar dynamical behavior of the COOH of the protonated dipeptide and tripeptide, this band is located in an identical position for the two peptides. Moreover, the slight asymmetry of this band is correctly reproduced by the calculations.

Based on the band assignments, the 3100−3500 cm^{-1} region can be separated into two parts. The 3300−3500 cm^{-1} frequency region is assigned to the stretches of the N−H groups of the tripeptide not involved in hydrogen bonds along the dynamics, i.e. the symmetric and antisymmetric stretch of the N-terminal amine NH_2, the stretches of the free N−H of the protonated N-terminal NH_3^+, and the stretches of the C-terminal amide N−H. The 3100−3300 cm^{-1} frequency domain is entirely related to the stretching bands of the N-terminal amide N−H group. As previously described, this amide group can be weakly hydrogen bonded to the amine N-terminal in the NH_2 tripeptide family (through a distorted H-bond) and also weakly hydrogen bonded to the C-terminal carbonyl of the peptide in the NH_3^+ family (again distorted H-bond because of steric hindrances). These H-bonds are therefore strong enough to induce the shift toward lower energy of the N-terminal N−H stretch in comparison to the positions of the free N−H groups. Note that the weak attraction of the N-terminal N−H with the carbonyl COOH extremity (over parts of the dynamics) is not strong enough to induce such a shift.

The 3300−3500 cm^{-1} part of the spectrum calculated for the NH_3^+ family is shapeless in comparison to the spectrum of the NH_2 family (Figure 5-A). In this later case, two nonoverlapping active bands can indeed be observed. As a consequence, the 3300−3500 cm^{-1} region of the experimental spectrum is better explained by the spectrum of the NH_2 family of the Ala_3H^+ peptide than by the spectrum of the NH_3^+ family. In contrast, the N-terminal N−H 3100−3300 cm^{-1} frequency domain is better explained by the superposition of spectra coming from the two families. This region is indeed composed of four main peaks that are organized within the same overall patterns in both NH_2 and NH_3^+ families of Ala_3H^+ (with the two higher frequency bands displaying higher intensities than the two lower frequency bands) but with significant band shifts. Hence, the bands of the NH_2 family are down shifted from the bands of the NH_3^+ family, by ∼80−100 cm^{-1} for the two higher frequency bands and by ∼30−40 cm^{-1} for the two lower frequency bands. As a consequence of these band shifts, the superposition of these bands in the final spectrum of Ala_3H^+ presented in Figure 5-C gives rise to a broadband where numerous subpeaks can be seen, nicely in agreement with the experimental vibrational patterns in the 3100−3300 cm^{-1} frequency region.

Though the band positions and band shapes of the spectrum of the folded Ala_3H^+ in the 3100−3500 cm^{-1} domain are different from the two unfolded families (note that there is only one dynamics acquired for the folded tripeptide versus three or four dynamics for each unfolded NH_2/NH_3^+ family, which could participate to these differences), their assignments follow the same lines as for the other two families, i.e. free N−H signatures at higher frequencies and H-bonded N−H signatures at lower frequencies. Note that all skeleton amide N−H stretches participate to the 3480 cm^{-1} band in the spectrum, while the free N−H of NH_3^+ give rise to the 3380 cm^{-1} band (Figure 5-B). The four peaks observed in the 3300−3100 cm^{-1} domain are related to the N−H group of NH_3^+ that was identified as forming a hydrogen bond with the neighboring N-terminal C═O group during the dynamics. This is different from the unfolded families and could be the reason for the different band shapes and intensities of the four bands in comparison to the four bands calculated for the unfolded families.

The final calculated spectrum presented in Figure 5-C, as the addition of the spectra of all families, i.e. unfolded/folded and NH_2/NH_3^+ N-terminus, therefore gives rise to several separate vibrational patterns of the N−H stretching motions, i.e. distinguishable subpeaks, which are in good agreement with the experiment. The overall shape is well reproduced by our calculations. The complex vibrational patterns of this large band are therefore a result of the local dynamics of the N−H groups in the different Ala_3H^+ families, in particular the dynamics of the H-bonded N−H which are different within the tripeptide families.

The 2800−3100 cm^{-1} domain is assigned to the C−H stretches arising from the methyls and the C_α−H groups of the tripeptide. Both CH_3 and C_α−H groups systematically participate in the two bands. All spectra calculated for all Ala_3H^+ families display two main intense bands located between 2900 and 3100 cm^{-1}, followed by a low intensity tail at lower frequency. Our final calculated spectrum therefore displays these properties in the 2800−3100 cm^{-1} domain, while a more featureless band can be observed in the experiment in the same region. There are nonetheless subpeaks that can be distinguished in the experiment which may be related to the separate peaks we obtain in our calculation. Note that these bands are shifted to higher frequency by ∼40 cm^{-1} with respect to the experiment.

As already observed for the Ala_2H^+ dipeptide, the vibrational signatures of NH_3^+ that are hydrogen bonded to the neighboring carbonyl in the NH_3^+ tripeptide family are strongly shifted to lower frequency compared to the other N−H stretches and appear over the extended 2000−2800 cm^{-1} domain. This breadth is entirely due to the vibrational anharmonicities and dynamics of the $N-H^+\cdots O{=}C$ H-bond at the finite temperature of the NH_3^+ family dynamics. Remarkably, the stretching of the protonated C−O−H in the NH_2 family is superimposed on the N−H^+ stretches of the NH_3^+ tripeptide family. It is therefore unfortunately not possible to distinguish both families using the stretching patterns of the H-bonded N−H^+ or C−O−H groups of the peptide, and it is also not possible to give a definite answer as to the location of the supplementary proton along the tripeptide chain. The strong frequency shifts result from the strong anharmonicities of these H-bonds.

The final spectrum of Ala_3H^+ calculated from the dynamics and presented in Figure 5-C agrees well with the experimental spectrum (regardless of band intensities that are indeed expected to give discrepancies). The 3560 cm^{-1} O−H stretch band of the C-terminal COOH of the Ala_3H^+ peptide is perfectly located at the experimental band position with a similar, slightly asymmetrical band-shape. The 3100−3500 cm^{-1} domain of the N−H stretching motions is overall well reproduced in our calculations, although displaying certain discrepancies with the experiment. The extent of the N−H stretch domain calculated here is identical to the experiment. The calculated 3300−3500 cm^{-1} higher frequency part is composed of a shoulder located at 3475 cm^{-1} which is located very close to the 3485 cm^{-1} shoulder in the experiment and a broadband located at 3390 cm^{-1} with a shoulder of low intensity at 3345 cm^{-1}. These two last bands correspond to the 3390 cm^{-1} and 3350 cm^{-1} bands in the experiment, though the 3350 cm^{-1} band is definitely more intense (but again, the calculated and experimental signals are not identical for intensities). Note that the appearance of the 3350 cm^{-1} shoulder in the final spectrum is entirely due to the active mode in the spectrum of the NH_3^+ family. The intense experimental 3435 cm^{-1} band unfortunately does not have a comparable intensity in our calculation. Instead, we have a shoulder located between 3430−3470 cm^{-1} in the final calculated spectrum: the low intensity of this band in our calculation arises from the average of the IR spectra of the NH_2 and NH_3^+ families, where this region has a featureless shape and intensity for the NH_3^+ family, ultimately leading here to the decrease of the intensities of the bands arising from the NH_2 family. The 3100−3300 cm^{-1} lower frequency part of the N−H stretch region displays the same broadband as in the experiment with the appearance of the characteristic subpeaks observed in the experiment. The four main subpeaks that can be distinguished in the experiment (∼3270, 3220, 3120, and 3075 cm^{-1}) can also be found in our calculation (∼3260, 3210, 3145, and 3115 cm^{-1}). Two of the frequencies are therefore only downshifted by 10 cm^{-1} from their experimental counterparts, while the two lower frequencies are shifted to higher frequency by 25−40 cm^{-1}. The double bands and low intensity tail calculated for the C−H stretches in the 2900−3100 cm^{-1} domain are shifted by +40 cm^{-1} from the experiment and are more structured than the experimental bands.

In Figure 5-D, we have reported the scaled harmonic spectra obtained from our previous investigation[13] for the four optimized geometries of lowest energy of Ala_3H^+. As can be immediately observed, the N−H broadband of the experimental spectrum is systematically associated with only two main intense harmonic bands, grossly separated by 200 cm^{-1} and 150 cm^{-1}, respectively, for the NH_2 and NH_3^+ families; hints of a third band located close to the ∼3490 cm^{-1} experimental band can also be seen, with a very low intensity. With these harmonic normal modes, the highest frequencies are related to free N−H groups of the optimized geometries and the lowest frequencies to the hydrogen-bonded backbone N−H. Though these interpretations roughly agree with what has been obtained in the present work from molecular dynamics simulations, one should admit that the IR spectrum extracted here from MD does offer vibrational details in the 3100−3500 cm^{-1} N−H domain that are completely missed by the harmonic calculations, even when adding the four harmonic spectra of Figure 5-D. Last but not least, C−H harmonic modes predicted around 3000 cm^{-1} have no intensity, while the anharmonic spectrum extracted from MD correctly predicts the intensity in this region.

The interpretation given here from MD simulations that the broad and complex N−H vibrational band comes from the intrinsic local dynamics of the N−H groups in the different conformers/isomers of Ala_3H^+, and in particular the breaking/forming of N−H hydrogen bonds, can only be achieved when performing molecular dynamics simulations. Scaled harmonic spectra will never be able to give a definite conclusive interpretation. Moreover, C−H band intensities do not show up correctly with harmonic spectra, while they are correctly obtained through anharmonic molecular dynamics.

Conclusions

We have chosen the two prototype small protonated polyalanines Ala_2H^+ and Ala_3H^+ in order to demonstrate that the peptides dynamical features should be taken into account to obtain a precise understanding of the relation between IR-MPD experimental features obtained at finite temperature and the underlying molecular structural and dynamical properties, including vibrational anharmonicities. We found that the spectra of Ala_2H^+ and Ala_3H^+ calculated from the

DFT-based Born−Oppenheimer dynamics performed in this work are in very good agreement with the experiments (Figures 4 and 5). We recall that no scaling factors nor translations have been applied to the calculated spectra. Once more, we recall that calculated and recorded IR-MPD intensities are not strictly comparable. Our calculations give an interpretation of the recorded vibrational patterns in terms of the dynamics of the gas-phase peptides at finite temperature.

In the case of Ala_2H^+, the conformational dynamics between two conformers of the peptide that mainly differ by a rotation of the COOH C-terminus is responsible for the broad bands in the NH/OH vibrational region. Though α_L/α_R conformational dynamics has been observed for the Ala_3H^+ peptide (when increasing the temperature of the dynamics), it does not have any influence in the N−H/O−H vibrational region. Instead, the local dynamics of the N-terminal backbone amide N−H group does give rise to the complex 3100−3500 cm^{-1} broad IR band, involving forming and breaking of hydrogen bonds at finite temperature. This cannot be grasped by static harmonic calculations as demonstrated by the comparison between harmonic static vibrational spectra and anharmonic dynamical spectra. This adds up to our previous works[12,14,15] where similar conclusions have already been reached. Though the static harmonic spectra may be useful in grossly establishing the "general" conformational features of the Ala_3H^+ protonated peptide from the N−H/O−H vibrational region, it fails in giving a convincing understanding of the complex N−H vibrational band in relation to the peptide conformation. Such understanding is only achieved when the dynamics of the peptide is taken into account. There are still some discrepancies though between the final spectrum extracted from the dynamics and the IR-MPD experimental signal, but we feel that the present work demonstrates once more the real need for the use of molecular dynamics simulations in order to interpret vibrational spectroscopy experiments performed at finite temperature.

We have shown that the calculated O−H stretch band of the C-terminal extremety of the Ala_2H^+ and Ala_3H^+ alanine peptide perfectly matches the experiments. This band is commonly located in both peptides as a result of the free O−H group dynamics in both molecules (not H-bonded). The calculated N−H band of Ala_2H^+ lacks part of the broadness of the experimental band (approximately half the width of the experiment), while the one of Ala_3H^+ reflects the more complex experimental features. The experimental N−H band encompasses the 3300−3500 cm^{-1} domain for Ala_2H^+ and extends to the 3100−3500 cm^{-1} domain for Ala_3H^+. As demonstrated with our dynamics, the 3300−3500 cm^{-1} frequency domain contains the stretching motions of free N−H groups within the di- and tripeptide and displays the same general shape for both peptides, i.e. showing two main subpeaks. In going from Ala_2H^+ to Ala_3H^+, the dynamics of the slightly hydrogen bonded N-terminal amide N−H group gives rise to the 3300−3500 cm^{-1} band. As we have shown, the subpeaks which make up this 200 cm^{-1} large band originate from weak interactions between the N-terminal and the neighboring amide N−H group and reflect the diversity of the local dynamics of the N−H H-bonding patterns within the different families of the tripeptide. This gives rise to different band positions of this amide N−H stretch, thus forming the numerous subpeaks that can be observed in both the experiment and the calculation. We have thus shown that the dynamics of the H-bonded N-terminal amide N−H give rise to the numerous subpeaks arising in the lower frequency part. This is in contrast with the results of Rizzo et al.[9] on longer peptide chains obtained at very low temperature (∼10−20 K), where the individual signatures of each N−H group along the chain can be distinguished among the vibrational signatures.

Band shapes are very well reproduced by our calculations. The slight asymmetry of the O−H band of Ala_3H^+ is obtained as well as the shoulder at high frequency of Ala_2H^+. More remarkably, the band shape of the N−H vibrations is very well generated by our calculations (though not broad enough for Ala_2H^+) and has no equivalence from the harmonic calculations (see for instance refs 13 and 34 and Figure 5-D in the present work). This is due to the natural broadening arising from the finite temperature of the calculations, the conformational dynamics of the molecules in the simulations, and all anharmonicities which are naturally taken into account in the present calculations. Unfortunately, the 3000 cm^{-1} C−H stretch band obtained from the calculations is composed of two separate bands (Ala_2H^+ and Ala_3H^+), while a more compact and shapeless band is observed in the experiments. The position of this band is also systematically shifted by ∼+40 cm^{-1} in our calculations. Interestingly, the anharmonic dynamics performed here give rise to an infrared active C−H band, while harmonic calculations predict no intensity.[13,34]

The final spectrum of Ala_3H^+ has been calculated as the sum of the individual spectra (each one averaged over a few dynamics) from three different peptide families. This summation is essential for the understanding of the broad and complex N−H band. If the 3300−3500 cm^{-1} region of this band may be more easily understood solely from the dynamics of the NH_2 family, this does not hold true for the 3100−3300 cm^{-1} region. There, the combination of signatures arising from the NH_2 and NH_3^+ families (including the folded one) is pivotal to get the long and more shapeless tail composed of subpeaks.

The present DFT-based BO molecular dynamics demonstrate once more the importance of taking into account *in a direct way* the finite temperature dynamics of flexible gas-phase peptides, in order to calculate and interpret gas-phase infrared spectra that are recorded at temperatures of 300−400 K. In the present investigation of Ala_2H^+ and Ala_3H^+, the dynamics are pivotal in relation to the N−H stretching motions. Taking into account the dynamics of the peptides directly allows understanding of the evolution of the shape and width of the N−H bands when increasing the size of the peptide. Our experiments[13] show that the N−H stretch domain continues to evolve with the increase of the peptide chain length, indicating, in view of the present calculations, that there is a change in the dynamics of the N−H amide groups for the longer chains, which is essential to understand in order to get a precise and definite picture of the

conformational dynamics of the gas-phase peptide. This is where our combined experiments and calculations are heading.

Acknowledgment. A.C. and M.-P.G. thank IDRIS (Orsay, France) for generous access to their computational facilities. M.-P.G. acknowledges support from Genopole-France through the program 'ATIGE' Action Thématique Incitative de Génopole. A.C. and M.-P.G. acknowledge the help of the group of J. Hutter for their help with the CP2K code. We are grateful to the Royal Society for a USA/Canada Research Fellowship (T.D.V.) and a University Research Fellowship (L.C.S.), to The Leverhulme Trust (T.B., L.C.S., Grant F/08788G), and to Linacre College (T.D.V.) and Corpus Christi College, Oxford (T.B., L.C.S.) for support.

Supporting Information Available: Details on the DFT-based molecular dynamics simulations performed in this work. This material is available free of charge via the Internet at http://pubs.acs.org.

References

(1) Graf, J.; Nguyen, P. H.; Stock, G.; Schwalbe, H. *J. Am. Chem. Soc.* **2007**, *129*, 1179.

(2) Hamm, P.; Helbing, J.; Bredenbeck, J. *Annu. Rev. Phys. Chem.* **2008**, *59*, 291.

(3) Woutersen, S.; Hamm, P. *J. Phys. Chem. B* **2000**, *104*, 11316.

(4) Abo-Riziq, A.; Crews, B. O.; Callahan, M. P.; Grace, L.; de Vries, M. S. *Angew. Chem., Int. Ed.* **2006**, *45*, 5166.

(5) Brenner, V.; Piuzzi, F.; Dimicoli, I.; Tardivel, B.; Mons, M. *J. Phys. Chem. A* **2007**, *111*, 7347.

(6) Chin, W.; Piuzzi, F.; Dimicoli, I.; Mons, M. *Phys. Chem. Chem. Phys.* **2006**, *8*, 1033.

(7) Chin, W.; Dognon, F. P. J. P.; Dimicoli, I.; Tardivel, B.; Mons, M. *J. Am. Chem. Soc.* **2005**, *127*, 11900.

(8) de Vries, M. S.; Hobza, P. *Annu. Rev. Phys. Chem.* **2007**, *58*, 585.

(9) Stearns, J. A.; Boyarkin, O. V.; Rizzo, T. R. *J. Am. Chem. Soc.* **2007**, *129*, 13820.

(10) Chellgren, B. W.; Creamer, T. P. *Proteins* **2006**, *62*, 411.

(11) Polfer, N. C.; Oomens, J.; Suhai, S.; Paizs, B. *J. Am. Chem. Soc.* **2007**, *129*, 5887.

(12) Grégoire, G.; Gaigeot, M.; Marinica, D.; Lemaire, J.; Schermann, J.; Desfrançois, C. *Phys. Chem. Chem. Phys.* **2007**, *9*, 3082.

(13) Vaden, T. D.; de Boer, T. S. J. A.; Simons, J. P.; Snoek, L. C.; Suhai, S.; Paizs, B. *J. Phys. Chem. A.* **2008**, *112*, 4608.

(14) Marinica, C.; Grégoire, G.; Desfrançois, C.; Schermann, J.; Borgis, D.; Gaigeot, M.-P. *J. Phys. Chem. A* **2006**, *110*, 8802.

(15) Gaigeot, M.-P. *J. Phys. Chem. A* **2008**, *112*, 13507.

(16) Allen, M.; Tildesley, D. *Computer simulation of liquids*; Oxford Science Publications: 1997.

(17) Frenkel, D.; Smit, B. *Understanding molecular simulations*, 2nd edition; Academic Press: 2002.

(18) McQuarrie, D. *Statistical Mechanics*; Harper-Collins Publishers: New York, 1976.

(19) Vuilleumier, R.; Borgis, D. *J. Chem. Phys.* **1999**, *111*, 4251.

(20) Tassaing, T.; Danten, Y.; Besnard, M.; Zoidis, E.; Yarwood, J.; Guissani, Y.; Guillot, B. *Mol. Phys.* **1995**, *84*, 769.

(21) Guillot, B. *J. Chem. Phys.* **1991**, *95*, 1543.

(22) Glover, W.; Madden, P. *J. Chem. Phys.* **2004**, *121*, 7293.

(23) Pavlatou, E.; Madden, P.; Wilson, M. *J. Chem. Phys.* **1997**, *107*, 10446.

(24) Madden, P.; Impey, R. *Chem. Phys. Lett.* **1986**, *123*, 502.

(25) Silvestrelli, P.; Parrinello, M. *J. Chem. Phys.* **1999**, *111*, 3572.

(26) Silvestrelli, P.; Bernasconi, M.; Parrinello, M. *Chem. Phys. Lett.* **1997**, *277*, 478.

(27) Bernasconi, M.; Silvestrelli, P.; Parrinello, M. *Phys. Rev. Lett.* **1998**, *81*, 1235.

(28) Gaigeot, M.-P.; Sprik, M. *J. Phys. Chem. B* **2003**, *107*, 10344.

(29) Gaigeot, M.-P.; Vuilleumier, R.; Sprik, M.; Borgis, D. *J. Chem. Theory Comput.* **2005**, *1*, 772.

(30) Gaigeot, M.; Martinez, M.; Vuilleumier, R. *Mol. Phys.* **2007**, *105*, 2857.

(31) Wu, R.; McMahon, T. B. *J. Am. Chem. Soc.* **2007**, *129*, 11312.

(32) Lucas, B.; Gregoire, G.; Lemaire, J.; Maitre, P.; Ortega, J.; Rupenyan, A.; Reimann, B.; Schermann, J.; Desfrancois, C. *Phys. Chem. Chem. Phys.* **2004**, *6*, 2659.

(33) MacLeod, N. A.; Simons, J. P. *Mol. Phys.* **2007**, *105*, 689.

(34) Vaden, T. D.; de Boer, T. S. J. A.; MacLeod, N. A.; Marzluff, E. M.; Simons, J. P.; Snoek, L. C. *Phys. Chem. Chem. Phys.* **2007**, *9*, 2549.

(35) Vaden, T. D.; de Boer, T. S. J. A.; Simons, J. P.; Snoek, L. C. *Phys. Chem. Chem. Phys.* **2008**, *10*, 1443.

(36) VandeVondele, J.; Krack, M.; Mohamed, F.; Parrinello, M.; Chassaing, T.; Hutter, J. *Comput. Phys. Commun.* **2005**, *167*, 103.

(37) *The CP2K developers group*. http://cp2k.berlios.de/.

(38) Becke, A. *Phys. Rev. A* **1988**, *38*, 3098.

(39) Lee, C.; Yang, W.; Parr, R. *Phys. Rev. B* **1988**, *37*, 785.

(40) Krack, M. *Theor. Chem. Acc.* **2005**, *114*, 145.

(41) Goedecker, S.; Teter, M.; Hutter, J. *Phys. Rev. B* **1996**, *54*, 1703.

(42) Hartwigsen, C.; Goedecker, S.; Hutter, J. *Phys. Rev. B* **1998**, *58*, 3641.

(43) Fischer, G. *Chem. Soc. Rev.* **2000**, *29*, 119.

(44) Mantz, Y.; Gerard, H.; Iftimie, R.; Martyna, G. *J. Am. Chem. Soc.* **2004**, *126*, 4080.

CT900057S